ORIGINAL ARTICLE

Force feedback in a piezoelectric linear actuator for neurosurgery

Danilo De Lorenzo[1]*
Elena De Momi[1,2]
Ilya Dyagilev[3]
Rudy Manganelli[4]
Alessandro Formaglio[4]
Domenico Prattichizzo[4,5]
Moshe Shoham[3]
Giancarlo Ferrigno[1,2]

[1]*Politecnico di Milano, Bioengineering Department, NearLab, Milano, Italy*

[2]*Istituto di Tecnologie Industriali ed Automazione, Consiglio Nazionale delle Ricerche, Milano, Italy*

[3]*Technion, Israel Institute of Technology, Mechanical Engineering Department, Medical Robotics Laboratory, Haifa, Israel*

[4]*University of Siena, Department of Information Engineering, Siena, Italy*

[5]*Istituto Italiano di Tecnologia, Genova, Italy*

*Correspondence to:
Danilo De Lorenzo, Politecnico di Milano, Bioengineering Department, NearLab, Piazza Leonardo Da Vinci, 32, 20133 Milano, Italy. E-mail: danilo.delorenzo@mail.polimi.it

Abstract

Background   Force feedback in robotic minimally invasive surgery allows the human operator to manipulate tissues as if his/her hands were in contact with the patient organs. A force sensor mounted on the probe raises problems with sterilization of the overall surgical tool. Also, the use of off-axis gauges introduces a moment that increases the friction force on the bearing, which can easily mask off the signal, given the small force to be measured.

Methods   This work aims at designing and testing two methods for estimating the resistance to the advancement (force) experienced by a standard probe for brain biopsies within a brain-like material. The further goal is to provide a neurosurgeon using a master–slave tele-operated driver with direct feedback on the tissue mechanical characteristics. Two possible sensing methods, in-axis strain gauge force sensor and position–position error (control-based method), were implemented and tested, both aimed at device miniaturization. The analysis carried out was aimed at fulfilment of the psychophysics requirements for force detection and delay tolerance, also taking into account safety, which is directly related to the last two issues. Controller parameters definition is addressed and consideration is given to development of the device with integration of a haptic interface.

Results   Results show better performance of the control-based method (RMSE <0.1 N), which is also best for reliability, sterilizability, and material dimensions for the application addressed.

Conclusions   The control-based method developed for force estimation is compatible with the neurosurgical application and is also capable of measuring tissue resistance without any additional sensors. Force feedback in minimally invasive surgery allows the human operator to manipulate tissues as if his/her hands were in contact with the patient organs. Copyright © 2011 John Wiley & Sons, Ltd.

Keywords   force feedback; force sensor; keyhole neurosurgery; robotic surgery

Introduction

During keyhole neurosurgery, small probes or electrodes are inserted with high accuracy in the brain through a small aperture in the skull (e.g. for biopsy, deep brain stimulation, stereo-EEG). Robotic systems can help such insertion with passive, active or semi-active operation. The former devices autonomously move to a predefined position (e.g. the probe's entrance pose) before locking and powering off. Examples are the Neuromate (Renishaw

Ltd, UK) and the ROSA™ (MedTech, France), which replace the stereotactic frame in conventional neurosurgery (1). Two active commercial devices, the NeuroDrive™ and the Alpha-Drive (Alpha-Omega, Nazareth, Israel) provide for surgical electrodes insertion for brain signal recording (2). Semi-active robotic systems complement the surgeon action, rather than replacing it, and can be tele-operated, i.e. the surgeon interacts with the remote slave robot through a master handling device (3). Tele-operated systems can convey tactile feedback with force feedback through a haptic interface as if the surgeon's hands were in direct contact with the patient (4). Force feedback is helpful during surgical needle advancement to detect local mechanical properties of the tissue and to distinguish between expected and abnormal resistance, for example, due to the unexpected presence of vessels. Transparency quantifies the fidelity with which the brain tissue properties are presented to and perceived by the operator (5). From the master side, transparency is related to the mechanical characteristics of the haptic interface (6) and is quantified in terms of the match between the impedance of the explored environment and the impedance transmitted to the operator (7), while for the slave side, transparency is related to the accuracy in the force measurement.

Devices for force measurement can be implemented by putting sensors on the actuator, on the instrument shaft or on the instrument tip (8). For example, in the LANS system (9), designed for performing biopsies and other neurosurgical interventions, a load cell is placed on the actuator, off-axis with respect to the tool. Integrating force sensors in-axis with the tip of a surgical tool is difficult owing to the constraints on size, geometry, biocompatibility, and sterilizability. Several attempts have been made to put sensors on grippers or on dexterous instruments for laparoscopy (10,11) and systems have been designed to measure forces of pulsating microvessels (12), but all these solutions are not actually suited to keyhole neurosurgery because of the size constraints.

Force feedback can be carried out also without the use of force sensors, through position–position control where the difference between the nominal and actual position of the slave robot allows an estimate of the resistance forces being exerted by the environment (13,14). In (15) the authors present a force feedback system in which the position error is detected and reflected as force to the master hand control. Results on accuracy in force measurement are not reported. If an accurate dynamic model of the actuator is known, accurate environment force estimates can be obtained (5,16,17). Control-based force estimation methods have clear advantages in terms of miniaturization and sterilization. It was also demonstrated (18) that the insertion force depends on the insertion velocity. Lateral vibratory actuation showed instead a decrease greater than 70% in insertion force during skin penetration (19).

In this framework, we evaluated the ability of a slave tele-operation system prototype (20), part of the ROBOCAST system (21), for biopsy probe insertion in

estimating, with two methods, the resistance to the advancement (force) experienced by a standard probe for brain biopsies within a brain-like material. The biopsy probe is inserted by a piezoelectric actuated inchworm device that is driven by the surgeon through an Omega haptic device (Force Dimension, CH). The system was tested using different gelatine samples, mimicking brain tissue and at different velocities for both proposed methods. The objective of the study was to allow the neurosurgeon to detect the interfaces between tissues with different mechanical impedance (e.g. owing to the presence of membranes or vessels walls) in order to stop the procedure if an unsafe situation was encountered. The force resolution for this task should match or exceed human sensing resolution (just-noticeable-difference, JND), which is around 7% (22,23), or human perception (24).

Materials and Method

Hardware and control scheme

As described in (20), the ROBOCAST system for brain biopsy includes:

(1) a linear piezoelectric actuator (LA, Figure 1), driven by an inchworm piezo-actuated motor with two clamps (the back, BC, and front clamp, FC) and one extension element (the pushing device, P). BC, FC and P are actuated by three multilayer piezoelectric devices (Noliac, DK) resulting in micrometric step advancement (20). The actuator is equipped with an optical encoder (LIK 41, Numerik Jena, Germany). The step frequency is 100 Hz. The velocity is regulated by the voltage applied to the pushing element, from 8 to 32 V (23.4 mV step-size);
(2) a haptic master device (HD) (Omega3, Force Dimension, CH);
(3) a force sensors (FS) that encompasses four strain gauges (SG) (4.1 × 5.7 mm – Vishay EA-06-031CE-350) glued to the BC element in a full-bridge configuration, sensing resistance during probe advancement (gauge factor 2.08, nominal resistance 350 Ω, excitation voltage 10 V, amplified with bandwidth 0–1 kHz and gain 250).

A proportional controller (PC), with gain K_p, was designed for the slave end-effector to track the master end-effector. The control scheme for the tele-operation system is represented in Figure 2. The X_{surg} position, input by the user to the Omega system, is rendered as X_m and then scaled times K_x to define the nominal probe tip position X_{Sm}. X_s is the actual tip position. V'_{cmd} is the nominal velocity, obtained by multiplying the position error $(X_{Sm} - X_s)$ by the gain K_p that was tuned to 70. This value allowed a wide bandwidth controller and avoided permanent saturation of the non-linear function f, which is the relationship between the nominal velocity
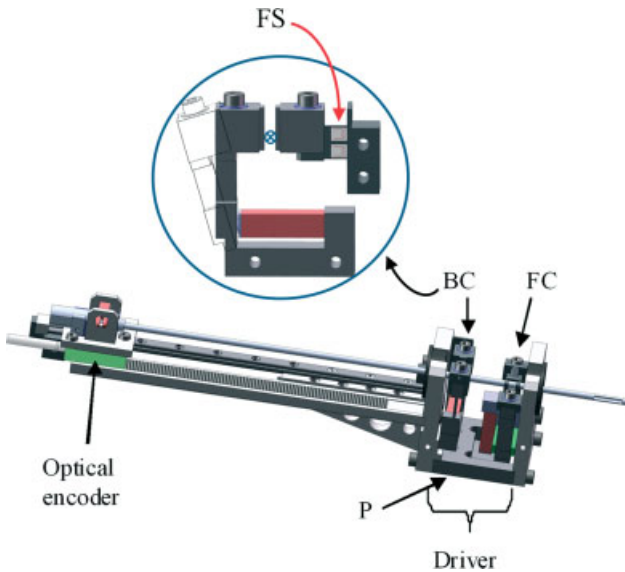
Figure 1. Slave linear driver of the ROBOCAST system (21). (1) linear piezoelectric actuator, with an inchworm piezo-actuated motor with two clamps (back, BC, and front clamp, FC) and one extension element (the pushing device, P); (2) linear optical encoder; (3) force sensors (FS) glued to the BC element
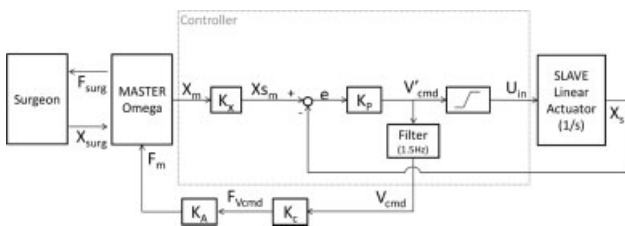

Figure 2. Control scheme: the surgeon input X_{surg} is translated into the reference position signal X_m, which is then multiplied by K_x (10). The error between the reference position signal Xs_m and the actual position X_s (measured by the linear encoder) is multiplied by the proportional coefficient of the controller (K_p). The resulting signal is converted into a voltage control signal ($U_{in} = 9.11 V'_{cmd} + 1.47$, as reported in (20), U_{in} is bounded between 8 and 32 V, and saturated below and above this interval) and input to the LA controller. The force estimated valued (V_{cmd}) is then multiplied by a calibration value (K_C), obtaining the force value (F_{Vcmd}), and then amplified ($K_A = 2$) and sent back to the surgeon (F_{surg})

(V'_{cmd}) and the input command ($U_{in} = f(V'_{cmd})$) and was experimentally determined in (20). The estimated value of the force is calibrated (K_C) in order to obtain the force values (F_{Vcmd}) and then further scaled (variable gain, K_A) before being passed to the surgeon through the rendering of the Omega (F_{surg}).

The resistance force experienced by the probe (f_{PROBE}) during insertion in the tissue is:

$$f_{PROBE} = f_{CLAMPING} + f_{ENVIRONMENT} + f_{HYDROSTATIC} \qquad (1)$$

where $f_{CLAMPING}$ is the friction due to the machining tolerances of the surgical instrument conflicting with the clamps of the LA; the push of the displaced gelatine ($f_{HYDROSTATIC}$) cannot overcome 0.78 mN and therefore

can be disregarded; $f_{ENVIRONMENT}$ is the actual brain resistance force (cutting force plus friction force).

The resistance force experienced by the probe (f_{PROBE}) was measured:

(1) using the calibrated force sensor FS;
(2) using the estimate provided by filtering the nominal velocity signal, F_{Vcmd}, which in turn is proportional to the difference between the nominal and actual tip position (X_{Sm} and X_S as shown in Figure 2).

The experimental protocol

Gelatine was prepared as a brain tissue surrogate. It was mixed in the ratio of 8%, 12%, and 16% with water. Similar mixtures were proposed in the literature for similar studies (25), since the insertion force of a surgical probe in them is similar to that observed in *ex vivo* brain tissue (26). A new gelatine sample was used for each test in order to avoid inhomogeneity due to old tracks. A Backlund biopsy probe (Elekta AB, SE, outer diameter 2.1 mm) was inserted repeatedly into the gelatine samples. Forward motion was tested, with the LA in vertical position, as in neurosurgical interventions. In order to analyse $f_{CLAMPING}$, an experiment was also conducted inserting the probe into a viscous liquid with a damping factor grossly comparable with gelatine (dishwashing gel), where $f_{ENVIRONMENT} = 0$.

Tests required a reference signal to compare quantitatively the force estimated using the two proposed methods with a ground truth. To this aim, a calibrated (R-square: 0.998) load cell (AB BOFORS KRK-2), with 5 mN accuracy, was positioned under the gelatine box to measure the reference signal (Figure 3). Five speeds of needle insertion were tested: 0.5, 0.8, 1.1, 1.5, and 2 mm/s. For each speed the following data were recorded at a sampling rate of 100 Hz:

(1) force signal from the force sensor FS (f_{FS});
(2) force signal from the load cell (f_{LC});
(3) nominal probe velocity (V_{cmd}), from which F_{Vcmd} was computed;
(4) probe position, measured by the optical encoder (X_S).

This protocol was applied to four types of sample: viscous gel and gelatine with 8%, 12%, and 16% concentration. Five trials were recorded for each speed and sample. Details of the experiments are reported in Table 1.

Data processing and analysis

The signal from the force sensor, f_{FS}, and F_{Vcmd} were both numerically processed with a low pass FIR filter (101 samples, $f_{cut} = 1.5$ Hz, Kaiser window). For each velocity and each gelatine sample, the load cell reference signal f_{LC} was used for calibrating f_{FS} and F_{Vcmd}; i.e. the least square linear model that minimizes the residual error
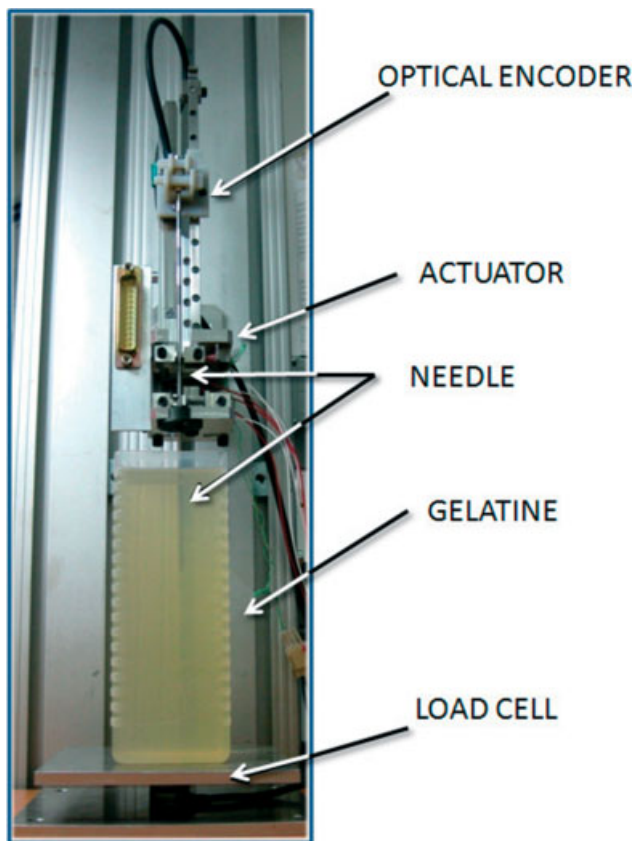
Figure 3. Positioning of the load cell under the gelatine sample

Table 1. Description of the tests

Test performed	Number of trials N = 5
Sample	Dishwashing gel
	8% gelatine
	12% gelatine
	16% gelatine
Nominal velocity	0.5 mm/s
	0.8 mm/s
	1.1 mm/s
	1.5 mm/s
	2 mm/s
Actuator position	Vertical
Stroke	60 mm

between four out of the five trials and the reference signal (f_{LC}) was computed. The model was then applied to the fifth trial set and the residual errors with respect to the reference (f_{LC}) computed. In order to gather a statistic of the measurement, the process was repeated five time ($j = 1, 5$ in Equations (2) and (3)) for each condition always 'leaving one trial out' of the five samples. The related RMSE values were:

$$RMSE_{f_{FS}}\,j = \sqrt{\frac{1}{Q}\sum_{i=1}^{Q}\left(f_{FS_i} - f_{LC_i}\right)^2}\quad j = 1, .., 5 \quad (2)$$

$$RMSE_{V_{cmd}}\,j = \sqrt{\frac{1}{M}\sum_{i=1}^{M}\left(F_{Vcmd_i} - f_{LC_i}\right)^2}\quad j = 1, .., 5 \quad (3)$$
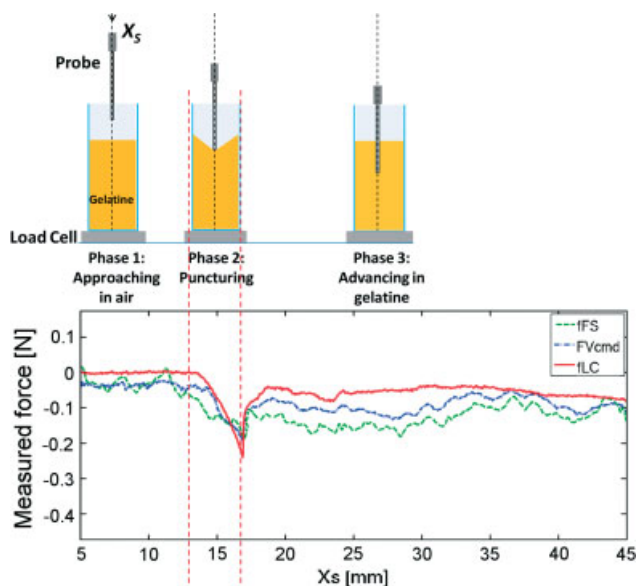

Figure 4. Example of signals acquired during probe insertion (12% gelatine at insertion velocity 0.8 mm/s)

where Q and M are the number of samples in each of the five acquisitions. Since the acquisitions performed at the same needle speed had the same number of samples, the geometric mean of the RMSE values was computed and taken as performance evaluation figure for each speed. This was an overall assessment of the measurement fidelity along all the recordings. In order to focus on the evaluation of the dynamic behaviour, the slopes of signals (f_{FS} and F_{Vcmd}) during the fast phases of the trials were measured. Figure 4 shows a typical time course of the data where a puncturing phase (Phase 2), with the highest frequency content of all the recordings, is easily recognized. The difference in the measurements obtained with the two methods (Δf_{FS} and ΔF_{Vcmd}), with respect to the reference load cell slope, was checked using the Kolmogorov–Smirnov test ($P < 0.05$).

Results

Results metrics and relevance are summarized in Table 2.

Gelatine characterization

Figure 5 shows the relationship between the environment force measured with the load cell (f_{LC}) and depth (X_S), for each insertion velocity, after the probe punched through the outer surface (phase 3 in Figure 4). The signals represented are the means of the data acquired using the same concentration of gelatine at constant temperature parameterized with the insertion speed. The velocity-dependent effect is clearly visible in all samples and increases with concentration. Figure 6 shows the slopes of the linear model fitted (with maximum RMSE 0.0084 N, as reported in Table 3) to the force–position relationship, reported in Figure 5, vs. the insertion

Table 2. Description and relevance of results

| Aim	Metrics	Relevance
Gelatine characterization	Force versus position/insertion velocity relationship	To characterize mechanical properties of the used material and compare results with literature
Clamping noise estimation	$F_{CLAMPING}$	To understand how results are influenced by the probe manufacturing
Accuracy of force estimation	RMSE OF f_{FS} and F_{Vcmd}	To choose the better method for force estimation
Response to fast changes	Slope of the puncturing phase	To estimate ability to render force variation at interfaces
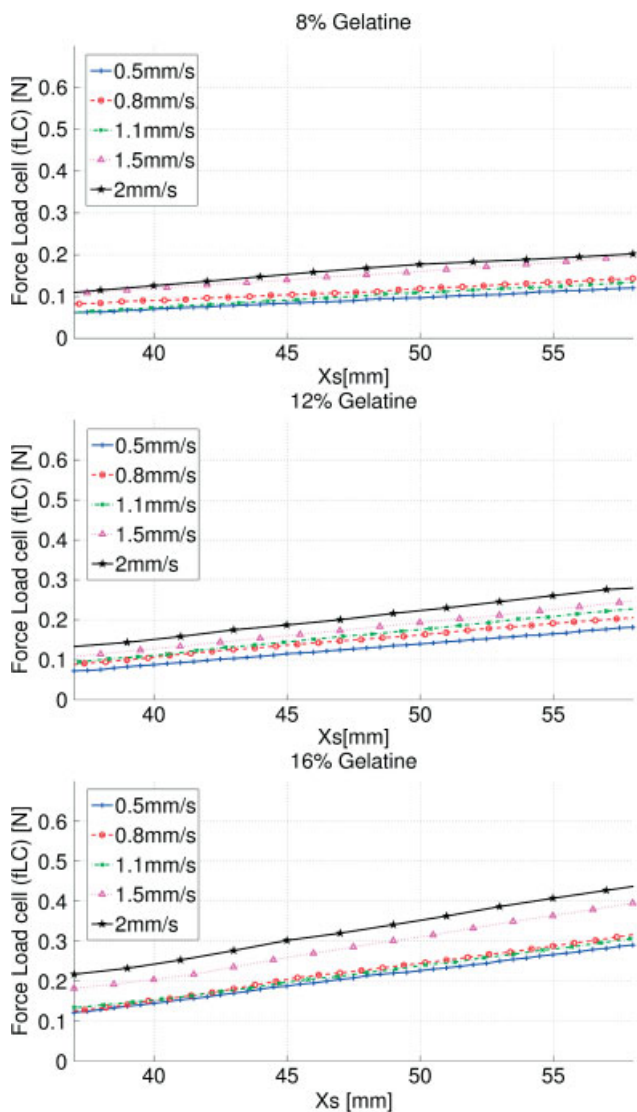
Figure 5. Force (f_{LC}) vs. probe insertion depth for different insertion velocities. Mean values are reported

speed. The slope increases with gelatine concentration (the viscosity coefficient increases). As shown, a good approximation to the function is provided by a scaled and shifted log curve for all the gelatine samples, as already observed in (12).

Clamping force estimation

Figure 7 shows f_{FS} and F_{Vcmd} measured inserting the probe in a viscous dishwashing gel. The data have been
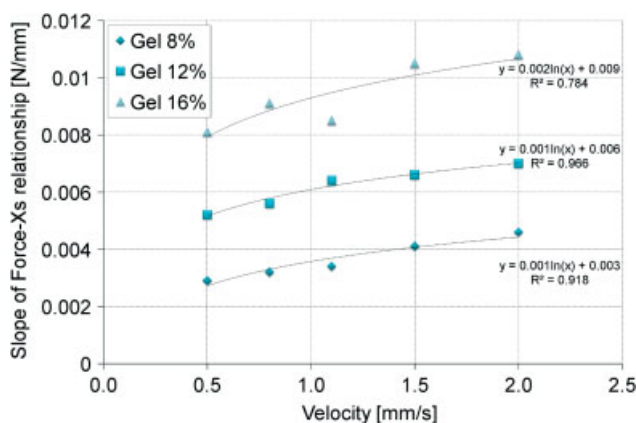

Figure 6. Slope of the force (f_{LC}) vs. position linear model for different insertion speeds. The slope is computed fitting a linear model to the data of Figure 5 and then averaged across different trials. Solid lines represent the log best fit

Table 3. RMSE residual of the fitting of a linear model to the force-position relation (reported in Figure 5)

Velocity	Gelatine[a] 8%	Gelatine[a] 12%	Gelatine[a] 16%
0.5 mm/s	0.0019	0.0017	0.0048
0.8 mm/s	0.0032	0.0034	0.0072
1.1 mm/s	0.0014	0.004	0.0049
1.5 mm/s	0.0032	0.003	0.0078
2 mm/s	0.0026	0.0064	0.0084

[a]N(Newton).

normalized to their maximum value. Mean and standard deviation of the five trials performed at 1.5 mm/s speed are plotted. Clamping force $f_{CLAMPING}$ estimated from f_{FS} shows several peaks and troughs, due to probe manufacturing imperfections, while F_{Vcmd} is clearly less affected by the probe imperfections (there is an offset of 0.01 N during the whole probe advancement). During these measurements, f_{LC} was nil.

Accuracy of the resistance force estimation

RMSE values of f_{FS} and F_{Vcmd} signals with respect to f_{LC} show comparable results, but the error does increase significantly with gelatine concentration. Considering F_{Vcmd}, 8% gelatine at 1.1 mm/s insertion velocity gave the best performances (RMSE less than 0.04 N). Maximum error was found with 16% gelatine at 1.5 mm/s (0.1 N). Since the resistant force experienced increases with speed
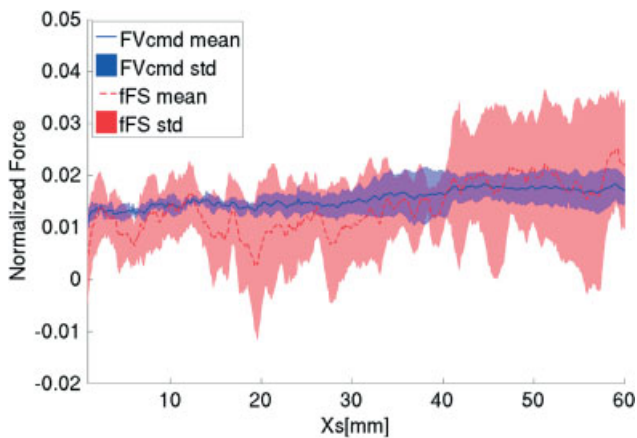
Figure 7. Clamping force ($f_{CLAMPING}$) vs. probe insertion depth estimated by f_{LC} and F_{Vcmd} in the dishwashing gel at 1.5 mm/s

Figure 9. Relative error during puncturing, measured as force signals slope difference with respect to the load cell (Median, 25th and 75th percentile)
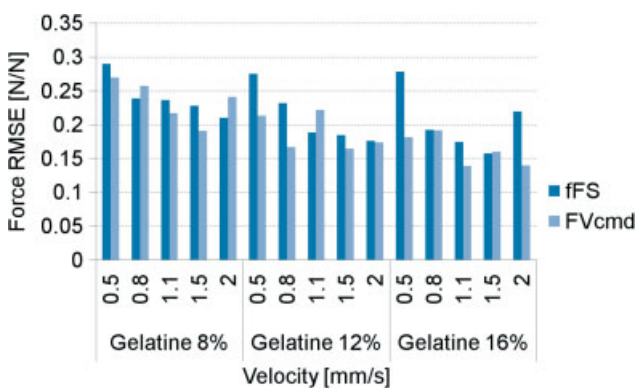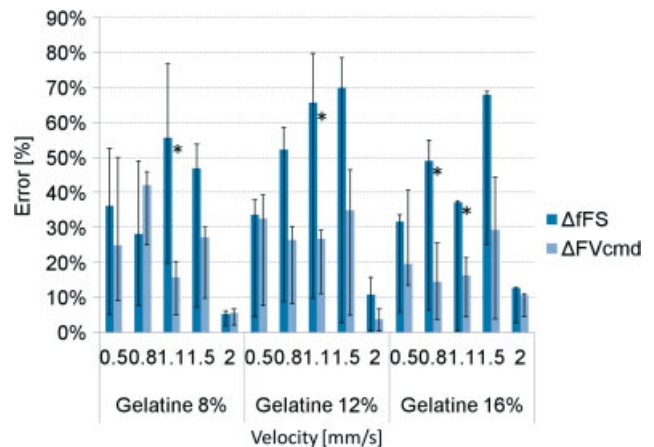

Figure 8. RMSE values of both force sensor f_{FS} and F_{Vcmd} signals normalized with respect to the maximum force

as well, the increase in RMSE does not change the full-scale resolution, as shown in Figure 8 where the RMSE values have been normalized to the maximum of the force measured in the trial. Similar results are obtained by normalising with respect to puncturing force.

Response to fast force changes

The fastest changes in force are experienced in Phase 2 (Figure 4). After the rupture of the outer membrane, the force reverts quickly close to the value measured in air and then linearly increases due to cutting force and to friction (Phase 3).

Figure 9 shows the sensing performance during the puncturing phase, expressed as signal slope differences, during Phase 2.

ΔF_{Vcmd} is significantly lower than Δf_{FS} at 1.1 mm/s and decreases as the insertion speed increases.

Discussion

In this paper we describe the experimental validation of a miniaturized tele-operated actuator for probe insertion in brain tissue, designed to provide the user with force feedback. In order to meet neurosurgical requirements, tip and shaft sensorization has been avoided to allow easy sterilizability and the use of standard (not modified) surgical tools. Owing to the small forces to be detected, off-axis sensors have also been avoided since the moment generated acting on the bearing stresses the device friction forces, hiding the signal. Furthermore one of the two measurement modalities (the position-position error) is sensor-less, in the sense that the deforming gauge is the tissue itself.

In the experiments a phantom made of brain-mimicking material was used, to test the system in controlled and repeatable conditions. Three different concentrations of gelatine in water were tested and the estimated forces were comparable with values reported in the literature using *in vitro* brain tissue (27,28). The results most similar to those with swine brain indentation experiments (maximum $f_{ENVIRONMENT}$ value 0.2 N at 2 mm/s insertion velocity) were obtained using 8% gelatine (12). The 16% gelatine showed the biggest variance since its stability is the most temperature-dependent. To control this problem, the number of trials was limited (N = 5) to avoid changing the properties of the samples at room temperature. Further tests on the brain-mimicking material behaviour are needed to estimate tissue damage, but they were beyond the scope of this work.

Brain resistance force, $f_{ENVIRONMENT}$, was computed by filtering the signals from the force sensor and the input velocity command (V'_{cmd}), proportional to the position error, which represented an estimate of the resistance force. Such estimates were compared with measurements made by the load cell and were seen to behave in almost in the same way. The sensor-less sensing modality (F_{Vcmd}), proved to be significantly better also during the puncturing phase when crossing the interface. By avoiding the need for any tip force sensor, the approach presented has clear advantages in terms of sterilization and miniaturization.

Because of the probe manufacturing processes (extrusion vs. rectification), the friction of the probe on the clamps, $f_{CLAMPING}$, can vary during advancement, and attempts to compensate this by gel measurements were unsuccessful. Also, during this latter experiment, F_{Vcmd} was shown to be the best estimator, for low bias and scatter.

System accuracy potentially satisfied the neurosurgery application requirements since the maximum error was 0.16 N on average. Using the 8% gelatine, which proved to replicate brain tissue mechanical properties, the system resolution (worst case) was around 20% of the puncturing force, independent of the insertion velocity. That value decreases in 16% gelatine. This result shows that the system can convey to the operator information on tissue discontinuities with a signal to noise ratio (>15 dB) close to the just noticeable difference (JND) (22–24).

Previous studies reported the effects of tip shape and needle diameter on soft human tissue (29,30) and show that rotation of the needle significantly decreases the force required to advance into the tissue (31). Also, an increase in needle insertion velocity could reduce the amount of tissue deformation (32). Forward–backward microvibrations (amplitude 6–10 μm, frequency ∼160 Hz), a by-product of the inchworm-like actuator used in this work, also help to avoid the probe sticking to tissue. Also it allows the velocity of each single step to be increased to 8 mm/s, limiting the total probe advance velocity (2 mm/s maximum). The other great advantage of the inchworm-like actuator is its small size and weight compared with its long stroke of 120 mm (theoretically unbounded) and high positional accuracy of 8 μm.

The proportional coefficient of the controller has been set as a trade-off between bandwidth ($f = K_p/2\pi$) and the accuracy of estimation of $f_{ENVIRONMENT}$: for high proportional gain (K_p) values, the tracking error converges towards zero. Furthermore this parameter cannot be too high otherwise the nonlinearity of the voltage driver would turn the continuous controller into a relay (two values only) controller. Stability of the control (Figure 2) is guaranteed by the existence of only one real pole in the feedback loop. Furthermore, the control signal (U_{in}) saturates below 8 and above 32 V, so the output variation is bounded. Further evaluation will be focused on tele-manipulation control, which was beyond the scope of this work. In particular the force feedback stability and accuracy during manual insertion will be taken into account considering the human operator in the control loop. Indeed, the controller pole frequency ($f = K_p/2\pi = 11$ Hz) may allow the surgeon to introduce instability in the outer loop. The problem is avoided by the low pass filter at 1.5 Hz cut-off on F_{Vcmd}. Such a low-pass filter also allows the cancelling of physiological tremor, which has typical frequency content from 10 to 30 Hz and amplitude of 100 μm RMS (33). The delay caused by filtering (500 ms) satisfies the requirements of the application since it allows probe advancement to be stopped within 1.3 mm (at 1.1 mm/s), if operator reaction time is 0.7 s, as reported in (34). Real-time implementation will lead to the use of an IIR filter requiring much less computational effort. Delay could also be reduced by adjusting the bandwidth and transition band.

Conclusion

The need to measure the force feedback in teleoperation has been demonstrated: the surgeon feels more comfortable and confident and performance, in terms of speed and accuracy, is enhanced (4–35). The importance of tactile sensation in increasingly technical neurosurgical procedures makes accurate haptic feedback an important element of simulation (36). Owing to its reduction of invasiveness, the possibility of using standard instrumentation, sterilizability (piezoelectric elements used can be sterilized in the autoclave) and overall size, the system proposed is suitable for neurosurgical applications. We also showed its capability to measure resistance without any additional sensors.

Acknowledgements

Conflict of Interest

All authors disclaim any financial and personal relationships with other people or organizations that could inappropriately influence (bias) their work.

References

1. Cossu M, Lo Russo G, Francione S, *et al.* Epilepsy surgery in children: results and predictors of outcome on seizures. *Epilepsia* 2008; Jan; **49**(1): 65–72.
2. Alpha Omega Engineering (Internet). (Accessed June 28, 2010).; Available from: http://www.alphaomega-eng.com/.
3. Sutherland G, Latour I, Greer A. Integrating an image-guided robot with intraoperative MRI: a review of the design and construction of neuroArm. *IEEE Eng Med Biol Mag* 2008; May; **27**(3): 59–65.
4. Hager GD, Okamura AM, Kazanzides P, *et al.* Surgical and interventional robotics: part III: surgical assistance systems. *IEEE Robot Automat Mag* 2008; Dec; **15**(4): 84–93.
5. Son HI, Bhattacharjee T, Lee DY. Estimation of environmental force for the haptic interface of robotic surgery. *Int J Med Rob Comp Ass Surg* 2010; Jun; **6**(2): 221–230.
6. Vlachos K, Papadopoulos E. Transparency maximization methodology for haptic devices. *IEEE/ASME Trans Mechatronics* 2006; Jun; **11**(3): 249–255.

7. Mahvash M, Okamura AM. Friction compensation for enhancing transparency of a teleoperator with compliant transmission. *IEEE Trans Robot* 2007; Dec; **23**(6): 1240–1246.

8. Puangmali P, Althoefer K, Seneviratne LD, *et al*. State-of-the-art in force and tactile sensing for minimally invasive surgery. *IEEE Sensors J* 2008; Apr; **8**(4): 371–381.

9. Rossi A, Trevisani A, Zanotto V. A telerobotic haptic system for minimally invasive stereotactic neurosurgery. *Int J Med Robotics Comput Assist Surg* 2005; Jan; **1**(2): 64–75.

10. Wagner CR, Howe RD. Force feedback benefit depends on experience in multiple degree of freedom robotic surgery task. *IEEE Trans Robot* 2007; Dec; **23**(6): 1235–1240.

11. Kuebler B, Seibold U, Hirzinger G. Development of actuated and sensor integrated forceps for minimally invasive surgery. *Int J Med Robotics Comput Assist Surg* 2005; **1**(3): 96–107.

12. Dario P, Hannaford B, Menciassi A. Smart surgical tools and augmenting devices. *IEEE Trans Robot Automat* 2003; Oct; **19**(5): 782–792.

13. Hannaford B. A design framework for teleoperators with kinesthetic feedback. *IEEE Trans Robot Automat* 1989; **5**(4): 426–434.

14. Lau HYK, Wai LCC. Implementation of position-force and position-position teleoperator controllers with cable-driven mechanisms. *Robot Comput Integr Manuf* 2005; Apr; **21**(2): 145–152.

15. Rosen J, Hannaford B, MacFarlane M, Sinanan M. Force Controlled and teleoperated endoscopic grasper for minimally invasive surgery – experimental performance evaluation. *IEEE Trans Biom Eng* 1999; Oct; **46**(10): 1212–1221.

16. Hacksel PJ, Salcudean SE. Estimation of environment forces and rigid-body velocities using observers. In Proceedings of the IEEE International Conference on Robotics and Automation, May 1994; San Diego, CA; 931–936.

17. Katsura S, Matsumoto Y, Ohnishi K. Analysis and experimental validation of force bandwidth for force control. *IEEE Trans Ind Electron* 2006; **53**(3): 922–928.

18. Crouch JR, Schneider CM, Wainer J, Okamura AM. A velocity-dependent model for needle insertion in soft tissue. *Med Image Comput Assist Interv* 2005; **8**: 624–632.

19. Yang M, Zahn JD. Microneedle insertion force reduction using vibratory actuation. *Biomed Microdevices* 2004; Sep; **6**(3): 177–182.

20. De Lorenzo D, Manganelli R, Dyagilev I, *et al*. Miniaturized rigid probe driver with haptic loop control for neurosurgical interventions. In *Biomedical Robotics and Biomechatronics (BioRob)2010*: Proceedings of the 3rd IEEE RAS and EMBS International Conference on Biomedical Robotics and Biomechatronics, Sept 2010; 26–29; Tokyo, Japan; 522–527.

21. De Momi E, Ferrigno G. Robotic and artificial intelligence for keyhole neurosurgery: the ROBOCAST project, a multi-modal autonomous path planner. *Proc IME Part H J Eng Med* 2010; May; **224**(5): 715–727.

22. Jones LA. Matching forces: constant errors and differential thresholds. *Perception* 1989; **18**: 681–687.

23. Pang XD, Tan HZ, Durlach NI. Manual discrimination of force using active finger motion. *Perception Psychophys* 1991; **49**(6): 531–540.

24. Shimoga KB. A survey of perceptual feedback issues in dexterous telemanipulation. I. Finger force feedback. In *Virtual Reality Annual International Symposium,* 18–22 Sep 1993; p. 263–270.

25. Engh J, Podnar G, Khoo S, Riviere C. Flexible needle steering system for percutaneous access to deep zones of the brain. In *Proceedings of IEEE Northeast Bioengineering Conference* 2006; 103–104.

26. Ritter RC, Quate EG, Gillies GT, *et al*. Measurement of friction on straight catheters in in vitro brain and phantom material. *IEEE Trans Biomed Eng* 1998; Apr; **45**(4): 476–485.

27. Howard MA III, Abkes BA, Ollendieck MC, *et al*. Measurement of the force required to move a neurosurgical probe through in vivo human brain tissue. *IEEE Trans Biomed Eng* 1999; Jul; **46**(7): 891–894.

28. Wittek A, Dutta-Roy T, Taylor Z, *et al*. Subject-specific non-linear biomechanical model of needle insertion into brain. *Comput Methods Biomech Biomed Eng* 2008; Apr; **11**(2): 135–146.

29. Shergold OA, Fleck NA. Experimental investigation into the deep penetration of soft solids by sharp and blunt punches, with application to the piercing of skin. *J Biomech Eng* 2005; Oct; **127**(5): 838–848.

30. Abolhassani N, Patel R, Moallem M. Needle insertion into soft tissue: A survey. *Med Eng Phys.* 2007; May; **29**(4): 413–431.

31. Hochman MN, Friedman MJ. An in vitro study of needle force penetration comparing a standard linear insertion to the new bidirectional rotation insertion technique. *Quintessence Int* 2001; **32**(10): 789–796.

32. Abolhassani N, Patel R, Moallem M. Trajectory generation for robotic needle insertion in soft tissue. In IEMBS 2004: Engineering in Medicine and Biology Society, 26th Annual International Conference of the IEEE, Sept 2004; 2730–2733.

33. Riviere CN, Gangloff J, de Mathelin M. Robotic compensation of biological motion to enhance surgical accuracy. *Proceedings of the IEEE* 2006; Sep; **94**(9): 1705–1716.

34. Dell'Acqua R, Turatto M. Cross-modal attentional deficits in processing tactile stimulation. *Perception Psychophys* 2001; **63**(5): 777–789.

35. Wagner CR, Howe RD. Force feedback benefit depends on experience in multiple degree of freedom robotic surgery task. *IEEE Trans Robot* 2007; Dec; **23**(6): 1235–1240.

36. Malone HR. Simulation in Neurosurgery: a review of computer-based simulation environments and their surgical applications. *Neurosurgery* 2010; Oct; **67**(4): 1105–1116.